RSC Advances

PAPER

View Article Online
View Journal | View Issue

Cite this: *RSC Adv.*, 2020, **10**, 1198

Polarization-enhanced photoelectric performance in a molecular ferroelectric hexane-1,6-diammonium pentaiodobismuth ($HDA\text{-}BiI_5$)-based solar device†

Xinyue Liu,[a] Ganghua Zhang,*[b] Mingjun Zhu,[b] Wenbo Chen,[a] Qi Zou*[a] and Tao Zeng*[bc]

Received 23rd December 2019
Accepted 26th December 2019

DOI: 10.1039/c9ra10839d

rsc.li/rsc-advances

Molecular ferroelectric $HDA\text{-}BiI_5$ has been utilized as the light-absorbing layer for organic–inorganic hybrid solar cells. Impressive polarization-induced enhancement of photoelectric performance has been achieved in the $HDA\text{-}BiI_5$-based solar device with a fast response time (~0.64 ms). This work may provide new perspectives for molecular ferroelectrics in photovoltaic and photodetector applications.

Introduction

Due to their outstanding photovoltaic performance, low-cost fabrication, and excellent mechanical flexibility, organic–inorganic lead halide perovskite solar cells have drawn enormous attention in recent years.[1–3] Their power conversion efficiencies (PCE) have grown tremendously from the initial 3.8% to more than 20% in just a decade,[4,5] but still suffer from the serious photocorrosion issue, toxic Pb and low stability in air. Due to the good structural tolerance, great efforts have been devoted to replacing the inorganic or organic portion with the aim to overcome such shortages of organic–inorganic lead halide perovskites. Ordinarily, there are two strategies for Pb-replacement. One is the utilization of the isovalent elements (such as Sn^{2+} and Ge^{2+}), which can maintain the perovskite-type framework but the stability is poor.[6,7] Another is choosing the heterovalent elements such as Bi^{3+} and Sb^{3+},[8–10] which can improve the stability but the conversion efficiency is a bit low. The substitution of other halide ions (Cl and/or Br) for unstable I^- ions has been demonstrated as an efficient route to promote the stability of organic–inorganic hybrid perovskites at the expense of efficiency.[11–14] Besides the inorganic portion, the replacement of the organic portion is also an efficacious way to enhance the performance of perovskite solar cells. For instance, the replacement of methylammonium ($CH_3NH_3^+$, MA) for formamidinium ($HC(NH_2)_2^+$, FA) enhanced the stability of the perovskite structure with an average PCE of 9.7% and the highest value of 14.2%.[15] Although great efforts have been devoted to the halide perovskites, the performance and stability are still hard to be satisfied simultaneously so far. Thus, it is extremely desired to explore more stable and efficient lead-free organic–inorganic hybrid compounds.[16]

On the other hand, many recent studies have demonstrated that the polarity of organic–inorganic halide perovskites likely plays a significant role in the excellent photovoltaic performance,[17,18] which is similar to the ferroelectric photovoltaic effects. Actually, since the abnormal photovoltaic effect with an impressively high voltage output, ferroelectrics with a narrow band gap (E_g) may have a bright future for solar-energy generation. It has been demonstrated that ferroelectric polarization is responsible for the high photovoltage and beneficial to the efficient separation of photoexcited electron–hole pairs.[19,20] Nevertheless, unlike the ferroelectric oxides, few studies have been devoted to the photoelectric performance of the molecular ferroelectrics. Considering the outstanding mechanical flexibility and intrinsic spontaneous polarization,[21,22] the molecular ferroelectrics could be a promising candidate toward organic–inorganic hybrid solar cells. Recently, hexane-1,6-diammonium pentaiodobismuth ($C_6H_8BiI_5N_2$, $HDA\text{-}BiI_5$) has been demonstrated as a room-temperature (RT) molecular ferroelectric material with the narrowest E_g (~1.89 eV) of the molecular ferroelectrics reported previously.[21] However, the photovoltaic properties of $HDA\text{-}BiI_5$ have never been verified, in spite of the visible-light absorption and room-temperature ferroelectric nature. Herein, we employed $HDA\text{-}BiI_5$ as a new kind of the light-absorbing layer for organic–inorganic hybrid solar cells. The solar cell device assembled by depositing $HAD\text{-}BiI_5$ film on the TiO_2/ITO glass substrate exhibits a remarkable photoelectric

[a]*Shanghai Key Laboratatory of Materials Protection and Advanced Materials in Electric Power, Shanghai University of Electric Power, Shanghai 200090, China. E-mail: qzou@shiep.edu.cn*

[b]*Shanghai Key Laboratory of Engineering Materials Application and Evaluation, Shanghai Research Institute of Materials, Shanghai 200437, P. R. China. E-mail: Zhangjiesss923@163.com; zengtao@srim.com.cn*

[c]*Advanced Science Research Laboratory, Saitama Institute of Technology, Okabe, Saitama 369-0293, Japan*

† Electronic supplementary information (ESI) available: Experimental details, EDS results, SEM images, and supplemental spectra. See DOI: 10.1039/c9ra10839d

effect with a fast response time less than 1 ms. The key factors affecting the photovoltaic performance of the (HDA-BiI_5)-based solar cell device have been also investigated systematically. Great photocurrent enhancement in (HDA-BiI_5)-based solar cell can be achieved by adjusting the ferroelectric polarization.

Experimental

Synthesis of HDA-BiI_5 crystals

The synthesis of hexane-1,6-diammonium pentaiodobismuth (HDA-BiI_5) was based on the reported literature.[21] All the reagents are of analytical grade and used without further purification. 5.9 g BiI_3 (10 mmol) and 1.16 g 1, 6-diaminohexane (10 mmol) were directly dissolved in an excess of HI solution (45% in water) at 363 K under nitrogen atmosphere. Single crystals of HAD-BiI_5 with micrometer dimensions were formed by cooling down slowly to room temperature.

Device fabrication

Normally, FTO and ITO are two most appropriate substrates used in photoelectric devices. Compared with FTO, the ITO substrate has the advantages of high electrical conductivity, good optical transparency, and well-established manufacturing process. Meanwhile, ITO substrate leads to more crystalline structure corresponding to the denser and smoother morphology which may be induced from the driven force provided by the recrystallization of ITO during annealing. Thus, ITO was selected as an appropriate substrate in this device fabrication.

The ITO glass substrates with the dimension of 1.0 cm × 2.0 cm were used after sequential ultrasonic cleaning with acetone, isopropanol, and DI water. And then, the substrates were treated with dry oven for 30 min.

The TiO_2 layer was prepared by spin-coating method. 2 mL titanium butoxide (AR, ≥98.0%), 1 mL diethanolamine (AR, ≥98.0%) and 0.0225 g polyethylene glycol (AR) were mixed by continuously stirring to obtain solution a. Then 0.6 mL acetic acid and 0.75 mL DI water were initially dissolved each other to prepared solution b. The two different kinds of solutions were then mixed with stirring. Subsequently, the mixed solution was left overnight. And then, 60 μL solution was spin-coated on the ITO substrate at 3000 rpm for 20 seconds, and then heated at 450 °C for 45 min. To further increase the contact area between the TiO_2 layer and the organic light-absorbing layer, the as-prepared TiO_2 thin-film was placed in a Teflon-lined container with a mixture of titanium butoxide (AR, 2 mL) and 1-butanol (AR, 28 mL). The hydrothermal reaction was conducted in a stainless-steel autoclave at 180 °C for 180 min in an oven. The hydrothermally retreated TiO_2 thin-film was then heated in a muffle furnace at 450 °C for 35 minutes. Thus, a compact TiO_2 layer was obtained with a total thickness of 7 μm.

The solution of HDA-BiI_5 was prepared by dissolving 500 mg HDA-BiI_5 into 0.4 mL *N*,*N*-dimethylformamide (AR, 99.8%). The compact HDA-BiI_5 layer was *in situ* deposited on the TiO_2 layer by spin-coating method and then drying at 120 °C for 30 min in a vacuum anneal furnace. The thickness of the HDA-BiI_5 layer was determined in the range of 10–70 μm. The overlap of the two ITO glasses, as the active areas, was about 1 cm^2.

Characterization

XRD patterns were obtained from a Rigaku D/Max-2000 diffractometer with Cu Kα radiation (λ = 1.5418 Å) at 40 kV, 100 mA at room temperature. The morphology and composition of the samples were determined by field-emission scanning electron microscope (SEM, JEOL JSM-7800F) equipped with an energy-dispersive spectrometer (EDS). Thermogravimetric analyses (TGA) of samples were tested by the thermal gravimetric analyzer (TGA 8000, PerkinElmer, USA). The optical properties of the samples were analyzed using a MAPADA UV-3100PC UV-Vis spectrophotometer. The photoelectric properties of the (HDA-BiI_5)-based solar devices were measured by an interactive source meter instrument (Model 2450, Keithley), under solar-light irradiations with a 500 W Xenon lamp.

Results and discussion

To confirm the purity and crystallinity of the HDA-BiI_5 powders and composite films, the powder XRD measurements were collected at room-temperature as given in Fig. 1a. All diffraction peaks of pristine HDA-BiI_5 powder and thin-film samples can be indexed to the orthorhombic system with the space group of $Pna2_1$ and the cell parameters of a = 15.076(1) Å, b = 14.307(1) Å and c = 8.644(1) Å, in according with the results reported previously.[21] The high quality and purity of the ITO/TiO_2/HAD-BiI_5 hybrid film were also revealed by XRD. The Bragg peaks of the hybrid film can be assigned to HDA-BiI_5, TiO_2 and Sn-doped In_2O_3 (from ITO), indicating that there is no introduction of other impurity in this assembled device. Fig. 1b shows the optical photograph of HAD-BiI_5 single crystal with a polyhedral shape and dark-red colour indicating the instinct visible-light

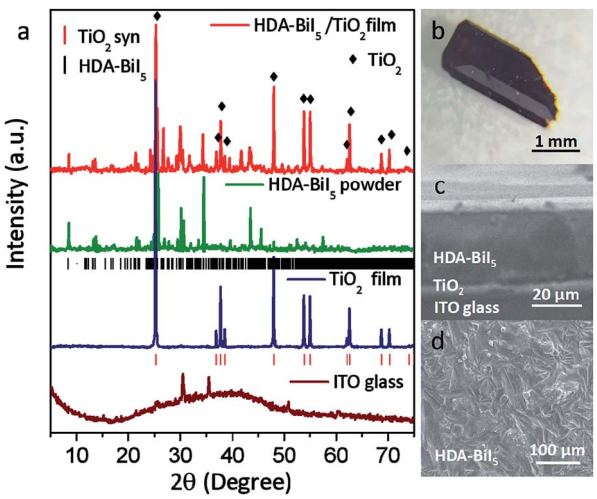

Fig. 1 (a) Comparison of XRD patterns: HDA-BiI_5 thin-film deposited on ITO/TiO_2 substrate (red), HDA-BiI_5 powder (green), TiO_2 thin-film (blue) and pure ITO glass substrate (wine). (b) Optical photograph of HDA-BiI_5 single crystal. (c and d) Cross-sectional and surface SEM images of the ITO/TiO_2/HDA-BiI_5 hybrid film.

absorption as discussed later. FE-SEM micrographs were performed to check the morphology of the thin-film device. Combining with the EDS analysis (Fig. S2†), it can be easy to visually distinguish the layered structure of the ITO/TiO_2/HAD-BiI_5 hybrid film from Fig. 1c, revealing the high quality of the assembled device that can predominantly affect the performance of solar cells as extensively demonstrated already.[23] From the SEM images of the top and side surfaces (see Fig. 1c and d), the as-prepared HDA-BiI_5 thin-film possesses high density and good crystallinity, suggesting the excellent stability of HDA-BiI_5 after annealing treatments.

The stability of HAD-BiI_5 has been also confirmed by the thermal gravity analysis (TGA) carried out in nitrogen atmosphere with a heating rate of 10 °C min^{-1}, and the result was showed in Fig. 2a. There was almost no weight loss below 300 °C, indicating good thermotolerance of HDA-BiI_5 thin-film annealing at 120 °C. Above 300 °C, the trend of the weight loss became more obvious and dropped sharply at 350 °C due to the decomposition of HDA-BiI_5, corresponding to the results reported previously.[21] In order to check the optical property of HDA-BiI_5 films, UV-Vis absorbance spectra have been measured at room temperature. As shown in Fig. 2b, all HDA-BiI_5 thin-film samples display an intense absorption at the onset of 650 nm, corresponding to a bandgap of 1.92 eV very close to the one reported previously (1.89 eV).[21] This narrow bandgap is matched well with the intrinsic red colour of the HDA-BiI_5 powder sample, suggesting the potential of HDA-BiI_5 as a light absorber for solar cells similar to $MAPbI_2Br$.[24] Moreover, the light absorption is definitely enhanced with increasing the thickness of HDA-BiI_5 films. The thicknesses of the HDA-BiI_5 films were estimated from the SEM images as shown in Fig. S3.†

Since the discovery of the visible-light photoelectric effect in $BiFeO_3$, the ferroelectric photovoltaics offers great potential for solar cell applications.[25–27] In order to assess the photoelectric performance of the molecular ferroelectric HDA-BiI_5, the photoelectric devices were assembled by spin-coating HAD-BiI_5 and TiO_2 sequentially on ITO glass substrate (Experimental details were given in ESI†). Fig. 3a depicts the schematic diagram of a device structure for (HDA-BiI_5)-based solar cell. Commonly, the TiO_2 thin-film layer has been extensively utilized in DSSCs to enhance the electron extraction and transportation to the cathode.[28–33] Thus, in this work, the TiO_2 thin-film layer was also been employed as an electron transport

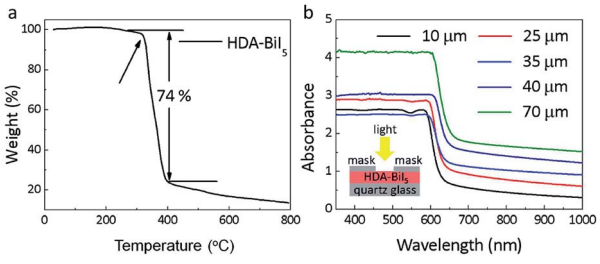

Fig. 2 (a) TGA data for HDA-BiI_5 crystals. (b) UV-Vis absorption spectra of HAD-BiI_5 films with various thicknesses. The inset schematically shows the measurement setup.

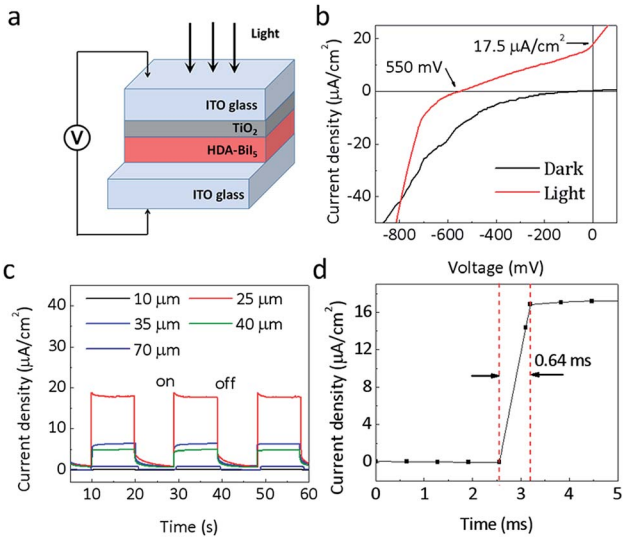

Fig. 3 (a) Schematic diagram of the (HDA-BiI_5)-based solar device. (b) *J–V* curves in dark and under sunlight simulator illumination at room temperature. (c) Zero-voltage photocurrent density with the variation of the HDA-BiI_5 film thickness following on–off sunlight simulator illumination. (d) Response time of (HDA-BiI_5)-based solar device.

layer. Fig. 3b shows the current–voltage (*J–V*) curves of the assembled devices. Under the illumination of a sunlight simulator, an obvious photoelectric response can be observed in (HDA-BiI_5)-based device with an open circuit voltage (V_{oc}) of 0.55 V and a short circuit current (J_{sc}) of 17.5 μA cm^{-2}, while the dark *I–V* curve shows negligible V_{oc} and J_{sc}. The present photovoltaic performance is comparable to the one reported in typical $MAPbI_3$-based devices without TiO_2 electron transport layer.[34,35] Moreover, it is far higher than that of the traditional ferroelectric oxide films, such as the well-known $BiFeO_3$ film made by pulsed laser deposition with a V_{oc} of 0.6 V and J_{sc} of only 1.3 μA cm^{-2}.[36] In fact, the morphology and crystallinity of TiO_2 thin-film layer can greatly affect the photoelectric properties of the DSSCs as always reported previously.[37–39] After hydrothermal retreatment for the as-prepared TiO_2 film, the photocurrent of the DSSCs increased significantly from 3.5 μA cm^{-2} to 17.5 μA cm^{-2} (see Fig. S5a†), which can be ascribed to the promoted density and larger surface area of the TiO_2 film treated hydrothermally. Associated with the light absorption and electronic transmission capability, the thickness of the HDA-BiI_5 film is also a critical factor to influence the performance of (HDA-BiI_5)-based solar cells. The current–time (*I–T*) curves of the HDA-BiI_5 films with various thicknesses were shown in Fig. 3b. With increasing the thickness of HDA-BiI_5 film, the J_{sc} increased sharply and reached up to a maximum of 17.5 μA cm^{-2} at 25 μm, and then turned down with further increasing the thickness of HDA-BiI_5 film (see Fig. S5b†). The improved photoelectric performance by the preferred film thickness can be attributed to the enhanced light-harvesting efficiency, improved charge-transport properties, and concomitantly reduced recombination loss as demonstrated previously.[40–42] Hence, the optimal thickness of the HDA-BiI_5 films was determined to be ~25 μm, and fixed for the further

comparison between other influence factors on the photoelectric performance of the (HDA-BiI_5)-based solar cell. Moreover, the response time of the (HDA-BiI_5)-based solar cell was presented in Fig. 3d. The fastest response time was reported about 0.72 ms in the $FAPbBr_3$ photodetector,[43] while our result was as low as 0.64 ms, indicating that this molecular ferroelectric would possess a bright prospect in the application of photodetector.

The long-term device stability of the (HDA-BiI_5)-based solar cell was also investigated in atmosphere condition held at room temperature under constant illumination. As shown in Fig. S5c,† it can be clearly found that the photocurrent degraded significantly over time. Without sealing, the (HDA-BiI_5)-based solar cell possessed a good long-term stability since its photocurrent decreased only by 14.3% of its initial value after 1 week. After three weeks, it still showed an obvious photoelectric response but the magnitude was extremely lower than the initial one. Thus, HDA-BiI_5 exhibited much more stability contrasting to the other organic–inorganic hybrid solar cells, such as $MAPbI_3$ which was quickly degraded and completely lost performance within several hours due to the hygroscopic nature of the methyl ammonium in a wet environment.[44] The excellent stability of HDA-BiI_5 should be attributed to the small size of Bi^{3+} which constructed a relatively stable crystal lattice.[45] This strategy for stabilizing the crystal lattice by replacing lead with chemically similar and suitable size atoms opened a promising route to prepare the molecular ferroelectric materials with good stability. Moreover, further improvement in the stability of (HDA-BiI_5)-based devices can be achieved by thoroughly sealed with epoxy resin or something similar.

Actually, the polarization has been verified to play a key role in the photoinduced charge separation and transmission in ferroelectric photovoltaics, which always lead to the enhanced photoelectric performance.[46–48] Even in the organic–inorganic hybrid perovskite solar cells, it is very likely that the polarization could be responsible for their outstanding photovoltaic performances.[49–51] Thus, after poling the HDA-BiI_5 film at different electric fields, the effect of ferroelectric polarization on the photoelectric properties of the (HDA-BiI_5)-based solar device has been detected under sunlight simulator illumination (Fig. 4). With increasing the poling electric field, the photocurrent density of the solar device showed a rapid increase till 5 V and followed by a fast drop up to 10 V for both positive and negative poling processes (see Fig. 4a and b), which confirmed the inherent relation between the polarization and photoelectric performance of the (HDA-BiI_5)-based solar cell. After poling at −5 V for 10 min, the photocurrent density reached a maximum of 92.4 μA cm^{-2}, which was about 5 times of the unpoled one of 17.5 μA cm^{-2}. However, positive poling switched the photocurrent direction and leaded to a maximum photocurrent density of −228.1 μA cm^{-2} after poling at 5 V for 10 min, which was about 13 times of the unpoled one. The switched photocurrent direction can be attributed to the opposite built-in field generated by the poling-induced alignment of domains as demonstrated previously in other ferroelectric photovoltaics.[52,53] The electronic band structure for ferroelectric solar cell based on HDA-BiI_5 under different polarization conditions was schematically shown in Fig. S6.† However, the J_{sc} decreased unpredictably with further increasing the poling field, indicating the complex competition between the ferroelectric polarization and PN junction in ferroelectric organic–inorganic hybrid solar cells. Further studies should be carried out to reveal all these issues.

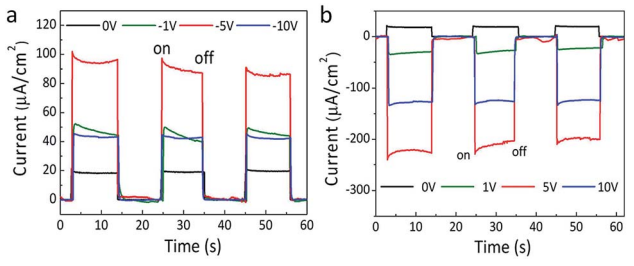

Fig. 4 The J–T curves of (HDA-BiI_5)-based solar device after negative (a) and positive (b) poling processes under sunlight simulator illumination.

Conclusions

In summary, molecular ferroelectric HDA-BiI_5 was utilized as the light-absorbing layer for the organic–inorganic hybrid solar cells for the first time. The (HDA-BiI_5)-based solar device exhibited a significant photoelectric effect with a V_{oc} of 0.55 V and a J_{sc} of 17.5 μA cm^{-2}. 13 fold enhancement in the photocurrent of the (HDA-BiI_5)-based device can be achieved by adjusting the ferroelectric polarization. Moreover, with a fast response time about 0.64 ms, (HDA-BiI_5)-based device also shows much brighter prospects in developing fast and sensitive photodetectors. In view all of these results, the utilization of molecular ferroelectrics is a novel promising strategy to explore new organic–inorganic hybrid solar cells with excellent photoelectric performances.

Conflicts of interest

There are no conflicts to declare.

Acknowledgements

This work was supported by the NSF of China Grant No. 51772184, Program of Shanghai Technology Research Leader Grant No. 17XD1420300, and LSD Project Grant No. 2016Z-04.

References

1 Y. Yang, L. Wu, X. Hao, Z. G. Tang, H. G. Lai, J. Q. Zhang, W. W. Wang and L. H. Feng, *RSC Adv.*, 2019, **9**, 28561–28568.
2 N. Ueoka, T. Oku and A. Suzuki, *RSC Adv.*, 2019, **9**, 24231–24240.
3 L. Theofylaktos, K. O. Kosmatos, E. Giannakaki, E. Kourti, D. Deligiannis, M. Konstantakou and T. Stergiopoulos, *Dalton Trans.*, 2019, **48**, 9516–9537.

4 D.-Z. Chen, X.-Yi. Li, A.-X. Su, H. Dong, S.-Z. Pang, W.-D. Zhu, H. Xi, J.-C. Zhang, C.-F. Zhang and Y. Hao, *Dalton Trans.*, 2019, **48**, 5292.
5 S. L. Chen, X. W. Zhang, J. J. Zhao, Y. Zhang, G. L. Kong, Q. Li, N. Li, Y. Yu, N. G. Xu, J. M. Zhang, K. H. Liu, Q. Zhao, J. Cao, J. C. Feng, X. Z. Li, J. L. Qi, D. P. Yu, J. Y. Li and P. Gao, *Nat. Commun.*, 2018, **9**, 4807.
6 Z. W. Xiao, Z. N. Song and Y. F. Yan, *Adv. Mater.*, 2019, 1803792.
7 W. Q. Liao, D. W. Zhao, Y. Yu, C. R. Grice, C. L. Wang, A. J. Cimaroli, P. Schulz, W. W. Meng, K. Zhu, R.-G. Xiong and Y. F. Yan, *Adv. Mater.*, 2016, **28**, 9333–9340.
8 S. S. Shin, J. P. C. Baena, R. C. Kurchin, A. Polizzotti, J. J. Yoo, S. Wieghold, M. G. Bawendi and T. Buonassisi, *Chem. Mater.*, 2018, **30**, 336–343.
9 F. Bai, Y. H. Hu, Y. Q. Hu, T. Qiu, X. L. Miao and S. F. Zhang, *Sol. Energy Mater. Sol. Cells*, 2018, **184**, 15–21.
10 B. Saparov, F. Hong, J.-P. Sun, H.-S. Duan, W. W. Meng, S. Cameron, I. G. Hill, Y. F. Yan and D. B. Mitzi, *Chem. Mater.*, 2015, **27**, 5622–5632.
11 N. J. Jeon, J. H. Noh, Y. C. Kim, W. S. Yang, S. Ryu and S. I. Seok, *Nat. Mater.*, 2014, **13**, 897–903.
12 M. Zhang, H. Yu, M. Q. Lyu, Q. Wang, J. H. Yun and L. Z. Wang, *Chem. Commun.*, 2014, **50**, 11727.
13 E. Edri, S. Kirmayer, M. Kulbak, G. Hodes and D. Cahen, *J. Phys. Chem. Lett.*, 2014, **5**, 429–433.
14 J. Hieulle, X. M. Wang, C. Stecker, D.-Y. Son, L. B. Qiu, R. Ohmann, L. K. Ono, A. Mugarza, Y. F. Yan and Y. B. Qi, *J. Am. Chem. Soc.*, 2019, **141**, 3515–3523.
15 G. E. Eperon, S. D. Stranks, C. Menelaou, M. B. Johnston, L. M. Herz and H. J. Snaith, *Energy Environ. Sci.*, 2014, **7**, 982–988.
16 X.-P. Cui, K.-J. Jiang, J.-H. Huang, Q.-Q. Zhang, M.-J. Su, L.-M. Yang, Y.-L. Song and X.-Q. Zhou, *Synth. Met.*, 2015, **209**, 247–250.
17 Z. Fan, J. X. Xiao, K. Sun, L. Chen, Y. T. Hu, J. Y. Ouyang, K. P. Ong, K. Y. Zeng and J. Wang, *J. Phys. Chem. Lett.*, 2015, **6**, 1155–1161.
18 W.-J. Xu, S. Kopyl, A. Kholkin and J. Rocha, *Coord. Chem. Rev.*, 2019, **387**, 398–414.
19 V. M. Fridkin, B. N. Popov and K. A. Verkhovskaya, *Phys. Status Solidi A*, 1977, **39**, 193–201.
20 C. C. Stoumpos, C. D. Malliakas and M. G. Kanatzidis, *Inorg. Chem.*, 2013, **52**, 9019–9038.
21 H.-Y. Zhang, Z. H. Wei, P.-F. Li, Y.-Y. Tang, W.-Q. Liao, H.-Y. Ye, H. Cai and R.-G. Xiong, *Angew. Chem., Int. Ed.*, 2018, **130**, 535–539.
22 Y.-M. You, W.-Q. Liao, D. W. Zhao, H.-Y. Ye, Y. Zhang, Q. H. Zhou, X. H. Niu, J. L. Wang, P.-F. Li, D. W. Fu, Z. M. Wang, S. Gao, K. L. Yang, J.-M. Liu, J. Li, Y. F. Yan and R.-G. Xiong, *Science*, 2017, **357**, 306–309.
23 Y. L. Wang, J. W. Wan, J. Ding, J.-S. Hu and D. Wang, *Angew. Chem., Int. Ed.*, 2019, **58**, 9414–9418.
24 Y.-M. Xie, C. Q. Ma, X. W. Xu, M. L. Li, Y. H. Ma, J. Wang, H. T. Chandran, C.-S. Lee and S.-W. Tsang, *Nano Res.*, 2019, **12**, 1033–1039.
25 S. Y. Yang, J. Seidel, S. J. Byrnes, P. Shafer, C.-H. Yang, M. D. Rossell, P. Yu, Y. H. Chu, J. F. Scott, J. W. Ager, L. W. Martin and R. Ramesh, *Nat. Nanotechnol.*, 2010, **5**, 143–147.
26 G. Zhang, H. Wu, G. Li, Q. Huang, C. Yang, F. Huang, F. Liao and J. Lin, *Sci. Rep.*, 2013, **3**, 1265.
27 G. Zhang, F. Liu, T. Gu, Y. Zhao, N. Li, W. Yang and S. Feng, *Adv. Electron. Mater.*, 2017, **3**, 1600498.
28 K. H. Ko, Y. C. Lee and Y. J. Jung, *J. Colloid Interface Sci.*, 2005, **283**, 482–487.
29 J. F. Qian, P. Liu, Y. Xiao, Y. Jiang, Y. L. Cao, X. P. Ai and H. X. Yang, *Adv. Mater.*, 2009, **21**, 3663–3667.
30 M. K. Nazeeruddin, P. Pechy, T. Renouard, S. M. Zakeeruddin, R. Humphry-Baker, P. Comte, P. Liska, L. Cevey, E. Costa, V. Shklover, L. Spiccia, G. B. Deacon, C. A. Bignozzi and M. Gratzel, *J. Am. Chem. Soc.*, 2001, **123**, 1613–1624.
31 I. Kartini, D. Menzies, D. Blake, J. C. D. da Costa, P. Meredith, J. D. Riches and G. Q. Lu, *J. Mater. Chem.*, 2004, **14**, 2917–2921.
32 M. Gratzel, *J. Sol-Gel Sci. Technol.*, 2001, **22**, 7–13.
33 Z. Q. Zhao, S. You, J. Huang, L. Yuan, Z. Y. Xiao, Y. Cao, N. Cheng, L. Hu, J. F. Liu and B. H. Yu, *J. Mater. Chem. C*, 2019, **7**, 9735.
34 A. Kojima, K. Teshima, Y. Shirai and T. Miyasaka, *J. Am. Chem. Soc.*, 2009, **131**, 6050–6051.
35 M. Z. Ge, C. Y. Cao, J. Y. Huang, S. H. Li, Z. Chen, K.-Q. Zhang, S. S. Al-Deyab and Y. K. Lai, *J. Mater. Chem. A*, 2016, **4**, 6772–6801.
36 H. Matsuo, Y. Noguchi and M. Miyayama, *Nat. Commun.*, 2017, **8**, 207.
37 Y. J. Kim, Y. H. Lee, M. H. Lee, M. H. Lee, J. H. Pan, Y. S. Choi, K. Kim, N.-G. Park, C. M. Lee and W. I. Lee, *Langmuir*, 2008, **24**, 13225–13230.
38 J.-W. Lee, T.-Y. Lee, P. J. Yoo, M. Grätzel, S. Mhaisalkar and N.-G. Park, *J. Mater. Chem. A*, 2014, **2**, 9251–9259.
39 M. Zukalova, A. Zukal, L. Kavan, M. K. Nazeeruddin, P. Liska and M. Gratzel, *Nano Lett.*, 2005, **5**, 1789–1792.
40 G. H. Zhang, Q. Zhang, Q. Y. Hu, B. H. Wang and W. G. Yang, *J. Mater. Chem. A*, 2019, **7**, 4019–4025.
41 J.-P. Correa-Baena, M. Anaya, G. Lozano, W. Tress, K. Domanski, M. Saliba, T. Matsui, T. J. Jacobsson, M. E. Calvo, A. Abate, M. Grätzel, H. Míguez and A. Hagfeldt, *Adv. Mater.*, 2016, **28**, 5031–5037.
42 Z. He, C. Zhong, X. Huang, W.-Y. Wong, H. Wu, L. Chen, S. Su and Y. Cao, *Adv. Mater.*, 2011, **23**, 4636–4643.
43 F. Y. Zhang, B. Yang, K. B. Zheng, S. Q. Yang, Y. J. Li, W. Q. Deng and R. X. He, *Nano-Micro Lett.*, 2018, **10**, 43.
44 A. F. Xu, R. T. Wang, L. W. Yang, V. Jarvis, J. F. Britten and G. Xu, *Chem. Commun.*, 2019, **55**, 3251.
45 X.-G. Zhao, J.-H. Yang, Y. H. Fu, D. W. Yang, Q. L. Xu, L. P. Yu, S.-H. Wei and L. J. Zhang, *J. Am. Chem. Soc.*, 2017, **139**, 2630–2638.
46 J. M. Frost, K. T. Butler, F. Brivio, C. H. Hendon, M. V. Schilfgaarde and A. Walsh, *Nano Lett.*, 2014, **14**, 2584–2590.

47 G. Zhang, J. Cao, G. Huang, J. Li, W. Yao and T. Zeng, *Catal. Sci. Technol.*, 2018, **8**, 6420–6428.
48 J. Li, G. H. Zhang, S. F. Han, J. W. Cao, L. H. Duan and T. Zeng, *Chem. Commun.*, 2018, **54**, 723.
49 Z. G. Xiao, Y. B. Yuan, Y. C. Shao, Q. Wang, Q. F. Dong, C. Bi, P. Sharma, A. Gruverman and J. S. Huang, *Nat. Mater.*, 2015, **14**, 193–198.
50 T. T. Sha, Y.-A. Xiong, Q. Pan, X.-G. Chen, X.-J. Song, J. Yao, S.-R. Miao, Z.-Y. Jing, Y.-M. You and R.-G. Xiong, *Adv. Mater.*, 2019, 1901843.
51 S. M. Vorpahl, R. Giridharagopal, G. E. Eperon, I. M. Hermes, S. A. L. Weber and D. S. Ginger, *ACS Appl. Energy Mater.*, 2018, **1**, 1534–1539.
52 B. Chen, J. Shi, X. J. Zheng, Y. Zhou, K. Zhu and S. Priya, *J. Mater. Chem. A*, 2015, **3**, 7699–7705.
53 B. Chen, X. Zheng, M. Yang, Y. Zhou, S. Kundu, J. Shi, K. Zhu and S. Priya, *Nano Energy*, 2015, **13**, 582–591.